Nanoscale Res Lett (2009) 4:400–408
DOI 10.1007/s11671-009-9254-5

NANO EXPRESS

Studies on Preparation of Photosensitizer Loaded Magnetic Silica Nanoparticles and Their Anti-Tumor Effects for Targeting Photodynamic Therapy

Zhi-Long Chen · Yun Sun · Peng Huang · Xiao-Xia Yang · Xing-Ping Zhou

Received: 13 November 2008 / Accepted: 8 January 2009 / Published online: 31 January 2009
© to the authors 2009

Abstract As a fast developing alternative of traditional therapeutics, photodynamic therapy (PDT) is an effective, noninvasive, nontoxic therapeutics for cancer, senile macular degeneration, and so on. But the efficacy of PDT was compromised by insufficient selectivity and low solubility. In this study, novel multifunctional silica-based magnetic nanoparticles (SMNPs) were strategically designed and prepared as targeting drug delivery system to achieve higher specificity and better solubility. 2,7,12,18-Tetramethyl-3,8-di-(1-propoxyethyl)-13,17-bis-(3-hydroxypropyl) porphyrin, shorted as PHPP, was used as photosensitizer, which was first synthesized by our lab with good PDT effects. Magnetite nanoparticles (Fe_3O_4) and PHPP were incorporated into silica nanoparticles by microemulsion and sol–gel methods. The prepared nanoparticles were characterized by transmission electron microscopy, X-ray diffraction, Fourier transform infrared spectroscopy and fluorescence spectroscopy. The nanoparticles were approximately spherical with 20–30 nm diameter. Intense fluorescence of PHPP was monitored in the cytoplasm of SW480 cells. The nanoparticles possessed good biocompatibility and could generate singlet oxygen to cause remarkable photodynamic anti-tumor effects. These suggested that PHPP-SMNPs had great potential as effective drug delivery system in targeting photodynamic therapy, diagnostic magnetic resonance imaging and magnetic hyperthermia therapy.

Keywords Targeting photodynamic therapy · Photosensitizer · Silica · Magnetic nanoparticles · Tumor

Z.-L. Chen (✉) · Y. Sun · P. Huang · X.-X. Yang · X.-P. Zhou (✉)
Department of Pharmaceutical Science and Technology, College of Chemistry and Biology, Donghua University, Shanghai 201620, China
e-mail: zlchen1967@yahoo.com

X.-P. Zhou
e-mail: xpzhou@dhu.edu.cn

Introduction

Photodynamic therapy (PDT) is an effective, noninvasive and nontoxic therapeutics for cancer, senile macular degeneration, actinic keratosis, port-wine stains, rheumatoid arthritis, and so on [1, 2]. After bio-distribution, photosensitizer (PS) administered systemically or topically is activated by light of appropriate wavelength and dosage. The activated PS transfers its excited-state energy to nearby oxygen molecular to generate reactive oxygen species, such as singlet oxygen ($^1O_2$) or peroxides inducing oxidative damage to target tissue and blood vessels that feed them [1–4]. Due to minimal invasion and nontoxicity, PDT provides patients, weak or failed in traditional therapy, opportunities to be treated painlessly and repeatedly.

However, the PDT efficacy is compromised by insufficient selectivity and low solubility. Although several methods including drug delivery systems were investigated [3–9], developing a PS delivery system for higher selectivity and less dark toxicity is still a challenge [5, 6].

Magnetic drug delivery system is a promising drug delivery system, which can be steered to the target tissue simply by an external magnetic field [10, 11]. Silica nanoparticles, easily prepared with desired size, shape and porosity, are water-soluble, stable and biocompatible. More importantly, silica nanoparticles are permeable to

small molecular such as singlet oxygen [4, 5], which is the key effector of PDT. Therefore, photosensitizer loaded silica nanoparticles are different from conventional delivery systems which need releasing of the loaded drug [9].

Previous investigations of fluorescent-magnetic nanoparticles mainly focused on the MRI imaging and fluorescence imaging for diagnosis; however, there are few studies on the multifunctional magnetic targeting drug delivery system for diagnosis and therapy [12, 13]. In the earliest study of magnetic targeting, a magnetic fluid was developed to which epirubicin was chemically bound to enable those agents to be directed within an organism by high-energy magnetic fields. In vitro and in vivo study of the epirubicin-magnetic fluid indicated biosafety and complete tumor response [10, 11], demonstrating the potential of magnetic targeting. Recently, the investigation of PS encapsulated magnetic silica nanoparticles (SMNPs) showed efficient cellular uptake [14] and obvious generation of singlet oxygen in vitro [15, 16], which indicated the potential of SMNPs as targeting drug delivery system.

Herein multifunctional PS encapsulated magnetic silica nanoparticles were strategically designed and synthesized, the silica shell of which can provide a porous environment for oxygen diffusion. 2,7,12,18-Tetramethyl-3,8-di-(1-propoxyethyl)-13,17-bis-(3-hydroxypropyl) porphyrin, shorted as PHPP, was used as photosensitizer, which was first synthesized by our lab with good PDT effects [17, 18]. The SMNPs were characterized by transmission electron microscopy, X-ray diffraction, Fourier transform infrared spectroscopy and fluorescence spectroscopy. The generation of singlet oxygen was monitored by RNO bleaching assay, and the photodynamic efficacy of the SMNPs to SW480 colon carcinoma cells was detected by MTT assay (Scheme 1).

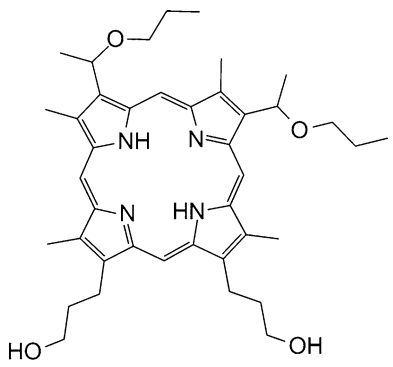

Scheme 1 Chemical structure of PHPP

Experimental Section

Materials

Ferrous(II) sulfate heptahydrate ($FeSO_4 \cdot 7H_2O$, 99%), ferric chloride hexahydrate ($FeCl_3 \cdot 6H_2O$, 99%), anhydrous ethanol (99.7%), ammonium hydroxide (25.2–28.0%), 1-butanol (99.8%), dimethyl sulfoxide (DMSO, 99.8%), tetrahydrofuran (THF, 99.9%), hydrochloric acid (36%) and oleic acid (99%) were purchased from Sinopharm Co. (China). Surfactant aerosol OT (AOT, 98%), tetraethylorthosilicate (TEOS, 99.99%), (3-mercaptopropyl) trimethoxysilane (MPS, 95%), *N*,*N*-dimethyl-4-nitrosoaniline (RNO, 99%), imidazole (≥99%), trypsinase (0.25%), and 3-(4,5-dimethylthiazol-2-yl)-2,5-diphenyltetrazolium bromide (MTT) were obtained from Aldrich. The PS PHPP was synthesized by our lab with purity ≥98%. SW480 cell was available in the cell store of Chinese Academy of Science. Other materials for cell culture, unless mentioned otherwise, were purchased from GIBCO. All the above-mentioned chemicals were used without any further purification.

Preparation of Fe_3O_4 Nanoparticles

In total, 2.51 g (9 mmol) $FeCl_3 \cdot 6H_2O$ and 1.25 g (4.5 mmol) $FeSO_4 \cdot 7H_2O$ were dissolved in 20 mL water. The solution was vigorously stirred, followed by adding 10 mL 1.5 mol L^{-1} $NH_3 \cdot H_2O$. The color of the solution was changed into black and the black solid produced was precipitated to the bottom. The Fe_3O_4 nanoparticles were obtained after the precipitants were washed for five times with 20 mL distilled water and 20 mL ethanol alternatively to remove unreacted chemicals.

Preparation of Silica-Based Fe_3O_4 Nanocarriers

In total, 1 g Fe_3O_4 nanoparticles and 10 g oleic acid were mixed with 10 mL ethanol. The suspension was refluxed for 30 min. Fe_3O_4/OA nanoparticles were obtained after the excess oleic acid was scoured off with ethanol by the magnetic decantation.

Micelles were prepared by dissolving 0.90 g AOT and 1600 μL 1-butanol in 40 mL doubly distilled water by vigorous magnetic stirring. A solution of 60 μL PHPP (15 mmol L^{-1}) in 1-butanol and 0.003 g Fe_3O_4/OA nanoparticles were added to above micellar system. After 30 min stirring, a new micellar system containing PHPP-Fe_3O_4/OA was formed. A total of 200 μL TEOS and 1.2 mL aqueous ammonia were added to the PHPP-Fe_3O_4/OA system prior to 1 h stirring. Then, 10 μL MPS was added, followed by continued 20 h stirring. The resultant

was treated by magnetic separation and washed with ethanol until no PS could be detected in the supernatant by UV–Vis spectroscopy. All the above-mentioned experiments were conducted at room temperature. The products were dried at 60 °C for 3 h in vacuum oven.

Characterization

The X-ray diffraction pattern of silica-based magnetic nanocarriers powders was obtained using D/max-2550PC (Geigerflex, Rigaku, Japan) with monochromated CuKα radiation operated at 40 kV and 100 mA. Transmission electron microscopy (TEM) was employed to determine the morphology and size of the aqueous dispersion of nanocarriers, using a HITACHIH-800 electron microscope, operating at an accelerating voltage of 200 kV. UV–Vis absorption spectra were recorded using a Jasco V-530 spectrophotometer, in a quartz cuvette with 1 cm path length. Fluorescence spectra were recorded on a HITACHIH FL-4500 spectrofluorimeter.

Encapsulation Efficiency Measurements

The UV–Vis measurements of the PHPP-SMNPs were carried out contrasted to other six groups: (a) PHPP; (b) Fe_3O_4 + PHPP; (c) PHPP + HCl; (d) Fe_3O_4 + HCl; (e) Fe_3O_4 + PHPP + HCl; (f) PHPP + lSMNPs + HCl. The amount of the mixed solvent was 0.1 mL the concentrated HCl and 2.9 mL ethanol. The absorbance at 409 nm was used to validate the PS presence and estimate the PS encapsulation efficiency. Each measurement was repeated three times.

The standard curve was established in the drug concentration range from 7.65×10^{-7} mol L^{-1} to 1.02×10^{-5} mol L^{-1}. Different concentrations of PHPP (7.65×10^{-7}, 2.55×10^{-6}, 5.10×10^{-6}, 7.65×10^{-6}, 1.02×10^{-5} mol L^{-1}) were mixed with 0.1 mL concentrated HCl and 2.9 mL ethanol. The samples were measured at 409 nm wavelength. Each experiment was repeated three times.

Detection of Singlet Oxygen

The PHPP-SMNPs in phosphate buffer (pH = 7.4) were irradiated in the presence of imidazole (10 mmol L^{-1}) and RNO (50 mmol L^{-1}). The RNO bleaching by $^1O_2$ was followed spectrophotometrically with observing the decrease in the 440 nm absorption peak of RNO as a function of irradiation time. The reaction mixture in a 1 cm spectrometric cuvette, placed at a distance of 12 cm, was continuously irradiated using 632.8 nm laser.

In Vitro Studies with Tumor Cells

Preparation of PHPP-SMNPs Solution

PHPP-SMNPs was diluted to 100 μmol L^{-1} with 0.5% carboxymethylcellulose sodium. The solution was then diluted with RPMI-1640 medium (supplemented with 100 U mL^{-1} penicillin, 10 U mL^{-1} streptomycin and 10% calf serum) using a dilution factor of 5 to varied concentrations: 0, 0.03, 0.13, 0.64, 3.20, 16.00, and 80 μmol L^{-1}.

Biosafety Assessment

SW480 carcinoma cells (3×10^3 cells per well) were seeded in 96-well plates and incubated overnight at 37 °C in a humidified 5% CO_2 atmosphere. After being rinsed with PBS (pH 7.4), the cells were incubated with 100 μL varied concentration of PHPP-SMNPs prepared above for 24 h at 37 °C in the dark under the same conditions. Rinsed with PBS, the cells were incubated another 48 h. Cell viability was determined by the colorimetric 3-(4,5-dimethylthiazol-2-yl)-2,5-diphenyltetrazolium bromide (MTT) assay. Cells were rinsed with PBS and then incubated with culture medium containing 0.5 mg mL^{-1} MTT reagent for 3 h. The medium was then removed and the formazan crystals formed were dissolved in 100 μL DMSO. The absorbance at 492 nm for each well was recorded by a microplate reader.

Photodynamic Activity Assay

Two plates were set up as dark control and experimental group for the MTT assay and these plates were seeded, exposed identically to the plates prepared for the biosafety assessment. The cells of experimental group were then rinsed again with PBS and immersed in 100 μL of fresh culture medium before being illuminated using a 488 nm argon-ion laser with energy density of 4.35 J/cm^2 from the underside of the culture plate. After 10 min illumination, cells were incubated 48 h in a 5% CO_2, 95% air humidified incubator at 37 °C. Dark control group keep identical to experimental group except illumination. Photodynamic activity assay was also determined by MTT assay as mentioned above.

Statistical Analysis

Cell viability was calculated using the following formula: average *A* value of experimental group/average *A* value of control group × 100%. Results were expressed as means ± SD. Comparisons between two groups were made by unpaired two-tailed Student's *t*-test using SPSS

15.0 software. *P*-value of less than 0.05 was taken to indicate statistical significance.

Results and Discussion

Preparation of Fe_3O_4 Nanoparticles

Fe_3O_4 nanoparticles, prepared by co-precipitation method [19, 20], were 10 ± 2 nm in diameter by measuring 200 randomly selected particles in enlarged TEM images, which agreed well with the value calculated from Scherrer Equation. Figure 1 shows the spherical morphology (Fig. 1a) and the characteristic peaks (Fig. 1b), which was compatible with the values of standard pattern. In addition to the dispersed and well-separated features, the formed Fe_3O_4 nanoparticles also exhibited some degree of aggregated morphology. The particles show an attraction to magnetic field, demonstrating the magnetic responsibility.

The Fe_3O_4 nanoparticles were coated with oleic acid according to the procedure described by Reimers [21, 22]. By adding oleic acid at melting point, the Fe_3O_4 nanoparticles were hydrophobized as illustrated in Fig. 2. The precipitate could be readily redispersed in the solvents such as cyclohexane, chloroform, or 1-butanol.

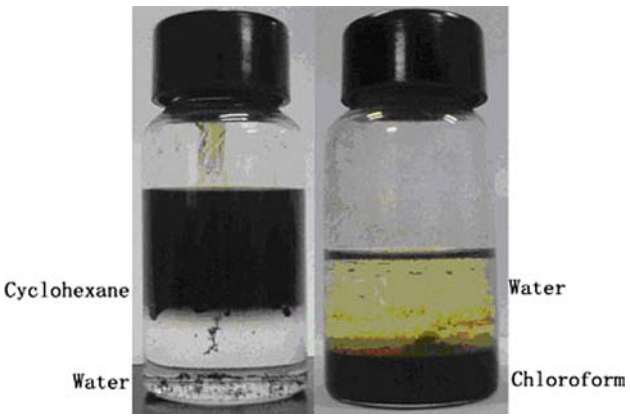

Fig. 2 The Fe_3O_4 nanoparticles hydrophobized by coating of oleic acid, dispersed in different system

Preparation of PHPP-SMNPs

Considering the size of the emulsion droplet is directly related to the final nanoparticle size, the formation of the emulsion is the key aspect. Emulsions can be classified in macroemulsions, microemulsions and miniemulsions (or nanoemulsions) The o/w microemulsion method is easy to scale up, it does not need high shear stress, and it is transparent and thermodynamically stable, with droplets mean sizes from 20 to 50 nm [23, 24]. So it is widely used for entrapment of hydrophobic compounds. Here, the o/w microemulsion method was combined with sol–gel method which was the classical approach to synthesize SiO_2 nanoparticles [25, 26]. The PHPP-SMNPs were prepared in the nonpolar core of AOT/1-butanol/water micelles, as shown schematically in a pictorial representation (Fig. 3). PHPP-absorbed Fe_3O_4/OA had priority to disperse in 1-butanol droplets redounding to form the nanocarriers.

Characterization of PHPP-SMNPs

TEM image (Fig. 4a) of PHPP-SMNPs showed that the PHPP-SMNPs were approximately spherical, sized in the range of 20–30 nm, but some agglomeration could be observed. Dynamic light scattering measurements were performed to study the behavior of a suspension containing PHPP-SMNPs. The hydrodynamic diameter of the nanocarriers was about 126 nm and the polydispersion was about 0.116, which verified the aggregates in the

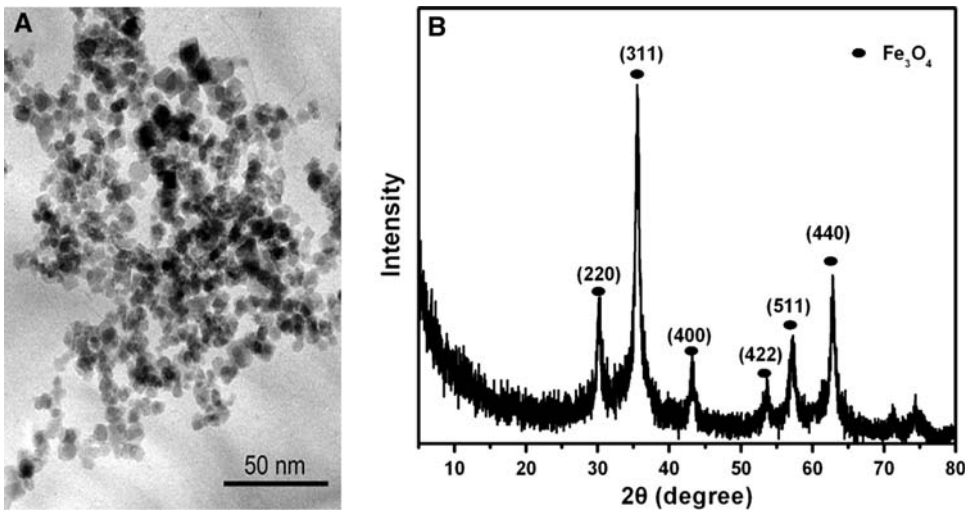

Fig. 1 TEM image (**a**) and XRD pattern (**b**) of Fe_3O_4 nanoparticles

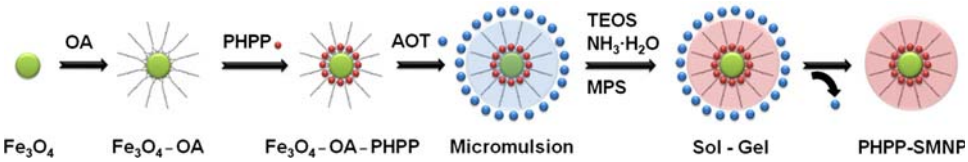

Fig. 3 Scheme depicting the synthesis and purification of (PHPP-Fe_3O_4/OA)/SiO_2

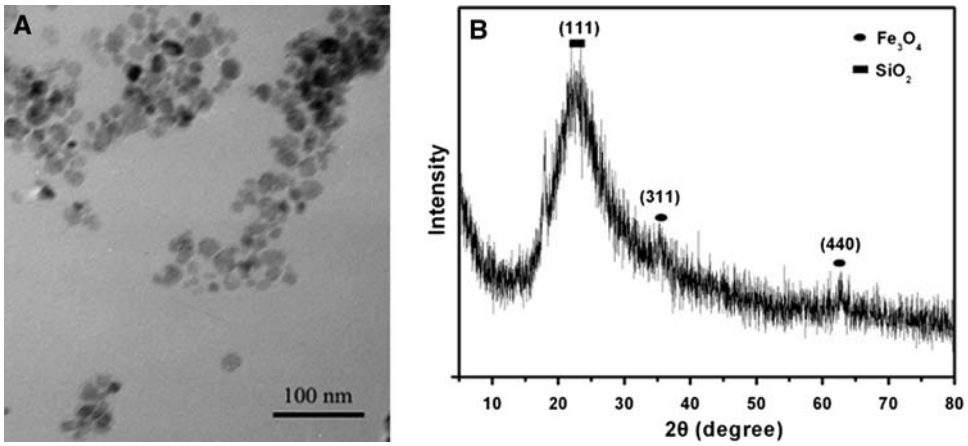

Fig. 4 TEM image (**a**) and XRD pattern (**b**) of PHPP-SMNPs

suspension of particles. These aggregates were not stable and could be easily redispersed by simply shake or sonication.

Figure 4b illustrates the XRD pattern of PHPP-SMNPs. The (111) peak is derived from the amorphous mesoporous silica spheres and the characteristic (311), and (440) peaks are typical of a cubic structure. The result showed that the crystallinity has not changed after encapsulation.

Figure 5 shows the typical FT-IR spectra of (a) PHPP, (b) SMNPs, and (c) PHPP-SMNPs. The bands C–H at 740 cm^{-1} (Fig. 5a) and C–O/C–N at 1079 cm^{-1} (Fig. 5c) indicated the encapsulation of the drug in the SMNPs. According to (b) and (c), it was found that the Si–O vibration absorption peak of the 1044 cm^{-1} shifted to 1079 cm^{-1}, which might be contributed to the integration of Si–O vibration absorption and C–O/C–N vibration absorption peak. The above facts suggested that PHPP was successfully wrapped in the SMNPs.

The photoluminescence peaks of PHPP were at 625 and 690 nm, as shown in Fig. 6. Figure 7 represents the fluorescence emission spectra of mother liquor and aqueous dispersion of the PHPP-SMNPs at same concentration. The emission signal from the PHPP in the PHPP-SMNPs was almost 20% of the all solution. Fluorescence intensity decreased significantly from (a) to (b), illustrating that PHPP was not completely encapsulated in the SMNPs.

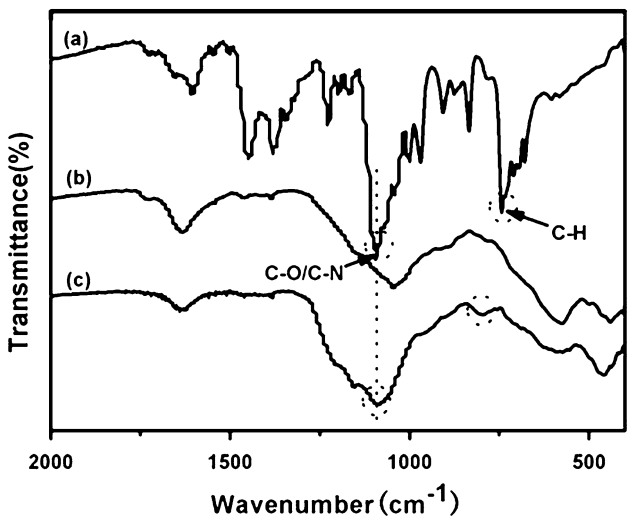

Fig. 5 FT-IR spectra of (a) PHPP, (b) (Fe_3O_4/OA)/SiO_2, and (c) (PHPP-Fe_3O_4/OA)/SiO_2

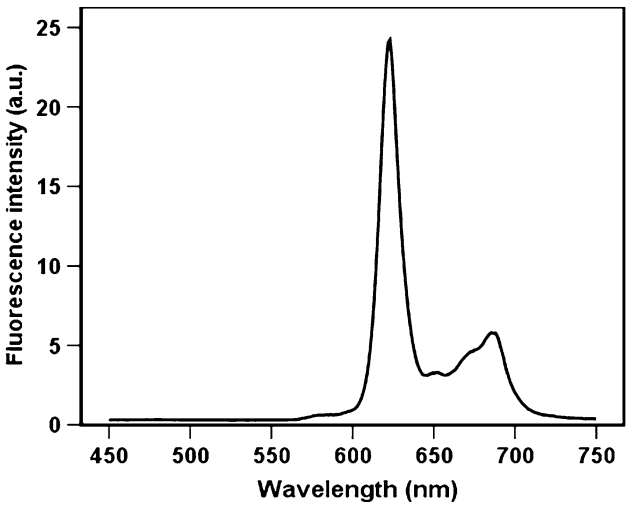

Fig. 6 Fluorescence emission spectra of PHPP. The excitation wavelength is 420 nm

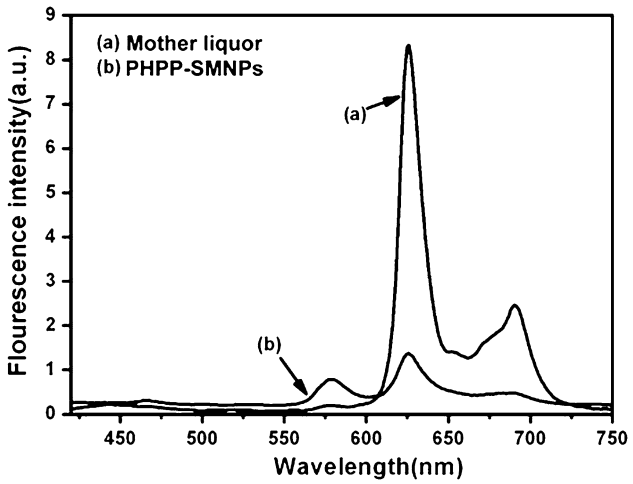

Fig. 7 Fluorescence emission spectra of (a) mother liquor and (b) PHPP-SMNPs

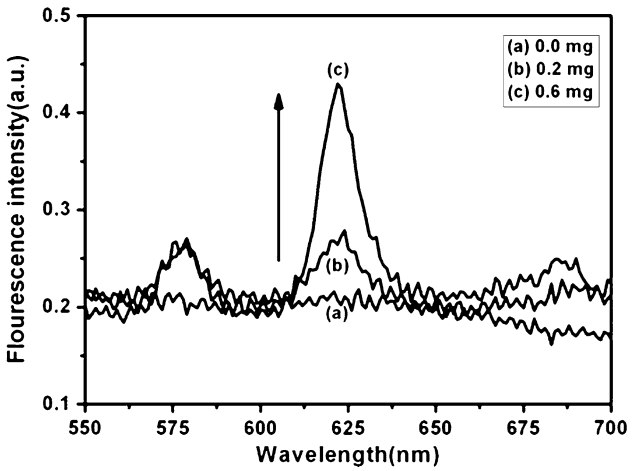

Fig. 8 Fluorescence emission spectra of (a) 0.0 mg, (b) 0.2 mg, and (c) 0.6 mg PHPP-SMNPs. The excitation wavelength is 420 nm

Figure 8 shows a concentration-dependent increase in photoluminescence signal, demonstrating the encapsulation of the PHPP again.

Encapsulation Efficiency Measurements

The amount of drug entrapped within PHPP-SMNPs was determined by dissolving PHPP-SMNPs into hydrochloric acid to destroy the Fe_3O_4 cores of PHPP-SMNPs for the release of PHPP. After ethanol addition, the absorbance of PHPP was detected and was performed by ultraviolet spectrophotometer at 409 nm.

Figure 9a shows the UV spectra of different substances in the 200–700 nm wavelength range, using ethanol as the solvent. The spectrum of PHPP (a) showed the special absorption peaks of PHPP at 399 nm. The increased absorption of PHPP and SMNPs mixture was caused by the

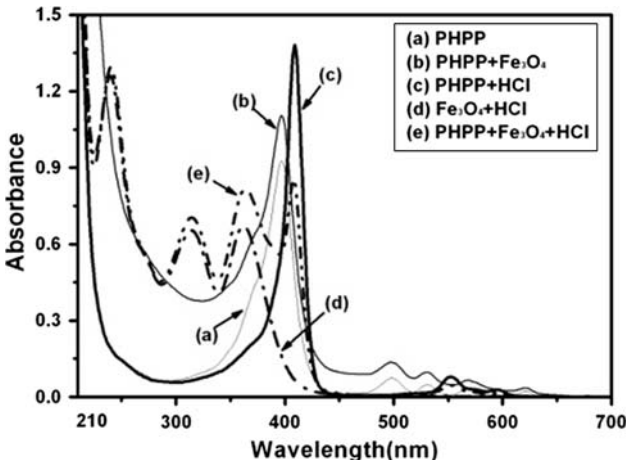

Fig. 9 UV spectra of (a) PHPP, (b) PHPP mixed with SMNPs, (c) PHPP dissolved in HCl and ethanol, (d) SMNPs dissolved in HCl and ethanol, and (e) SMNPs and PHPP dissolved in HCl and ethanol

absorption of SMNPs. The reaction of PHPP with HCl caused a red shift of the special absorption peak of PHPP from 399 to 409 nm (c). Spectrum (d) indicated absorptions of SMNPs and HCl at 240, 314, and 364 nm, demonstrating that the 240, 314, and 364 nm peak of the spectrum (e) attributed to SMNPs and HCl. Therefore, the 409 nm was the characteristic absorption peaks of PHPP with or without SMNPs.

The PHPP-SMNPs treated with HCl were detected by UV–Vis spectrophotometer and the spectrums are displayed in Fig. 10.

The standard curve had a good linear relation ($r = 0.99905$) within the range of 7.65×10^{-7} to 1.02×10^{-5} mol L^{-1}, described by the following typical equation: $Y = 0.04447 + 0.02571x$ (see Fig. 11). PHPP encapsulation efficiency was 20.8%, estimated by the typical equation.

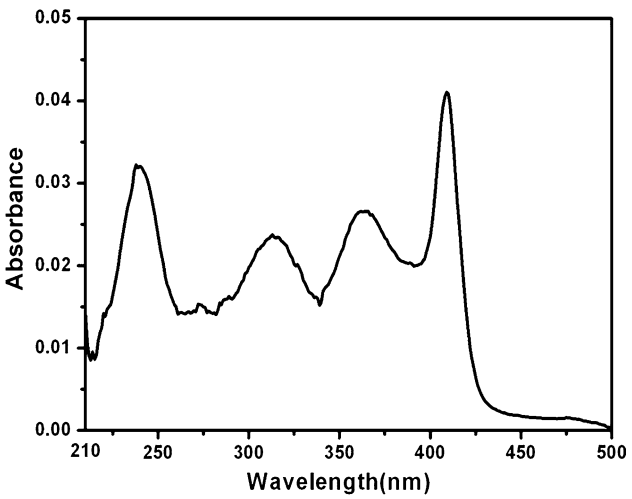

Fig. 10 UV spectra of the PHPP-SMNPs treated with HCl and ethanol

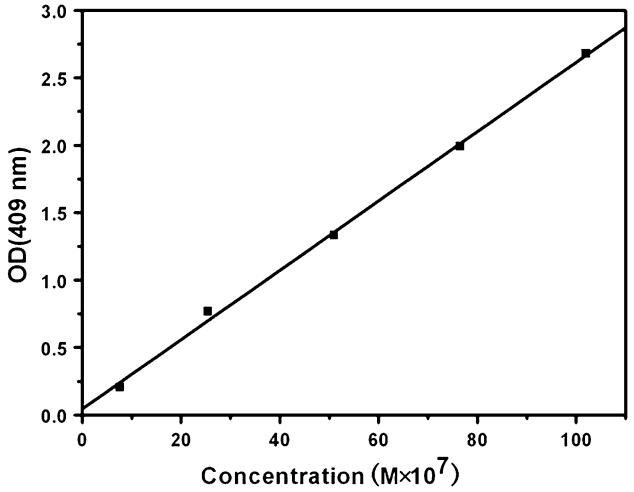

Fig. 11 The standard curve of PHPP dissolved in HCl and ethanol, measured at 409 nm. Typical equation: $Y = 0.04447 + 0.02571x$ (where x is the concentration and Y is the absorbance)

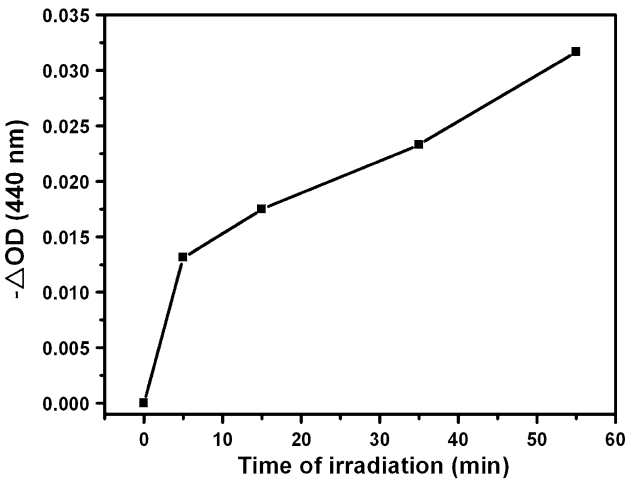

Fig. 12 Photosensitized RNO bleaching measured at 440 nm as a function of irradiation time

Detection of Singlet Oxygen

The *N*,*N*-dimethyl-4-nitrosoaniline (RNO) was used as an indicator for photo-induced singlet oxygen with imidazole as a chemical trap for singlet oxygen [27–29]. The principle of this method is shown in the following formula:

$$^1O_2 + \text{imidazole} \rightarrow [\text{imidazole} - {}^1O_2]$$

$$[\text{imidazole} - {}^1O_2] + \text{RNO} \rightarrow \text{RNO}_2 + \text{Products}$$

The bleaching of RNO by $^1O_2$ was followed spectrophotometrically with observing the decrease in the 440 nm absorption peak of RNO as a function of irradiation time.

A decrease in the 440 nm absorption peak of RNO was caused by the Fe_3O_4 nanoparticles without irradiation. So a 24 h aging of the PHPP-SMNPs and RNO system was necessary prior to detecting the $^1O_2$ productivity, until the absorption of RNO at 440 nm did not decline. The system was irradiated. The continued decrease at 440 nm absorption peak was caused by the significant generation of $^1O_2$ released from the PHPP-SMNPs (Fig. 12), indicating the potential for efficient PDT.

In Vitro Studies with Tumor Cells: Cellular Uptake, Biosafety Assessment and Photodynamic Activity Assay

Intracellular Uptake

As an essential tool in material science and biology, fluorescence microscopy demonstrates the ability to monitor the precise location of intracellular fluorescence materials excited by light of specific wavelengths, as well as their associated diffusion coefficients, transport characteristics, and interactions with other biomolecules. To test the intracellular uptake of PHPP-SMNPs, fluorescence imaging was performed on human SW480 colon carcinoma cells after incubation with 50 μmol L^{-1} PHPP-SMNPs for 4 h in cell culture incubator. As shown in Fig. 13, PHPP-SMNPs were taken up by SW480 cells and showed significant intracellular fluorescence (extra nuclear) compared to unincubated cell. As the PDT effects depend on the uptake of PS by tumor cells, the intense fluorescence of intracellular PHPP-SMNPs, related to the PS concentration, predicted an available obvious PDT effects. Subcellular distribution of PHPP-SMNPs in the cytoplasm primarily demonstrated slight effects on DNA.

Biosafety Assessment

Biosafety assessment was essential to evaluate the potential application of silica nanoparticle in clinics. Here, MTT assay was performed to detect the dark toxicity of PHPP-SMNPs. No obvious dark toxicity of PHPP-SMNPs on SW480 carcinoma cells was detected within 0.03–80 μmol L^{-1} concentration range in comparison with control (Fig. 14a). In addition, negligible cell death and physiological state changes of SW480 cells treated with highest dosage of PHPP-SMNPs were observed in Fig. 14b. It could be predicted that the PHPP-SMNPs had minimal, if any, impact on cellular functions, which indicated the low dark toxicity and good biocompatibility.

In Vitro Photodynamic Efficacy

Likewise, the MTT assay was performed to examine the phototoxicity of PHPP-SMNPs to SW480 colon carcinoma cell lines, which indicated the PDT efficacy in vitro [30].

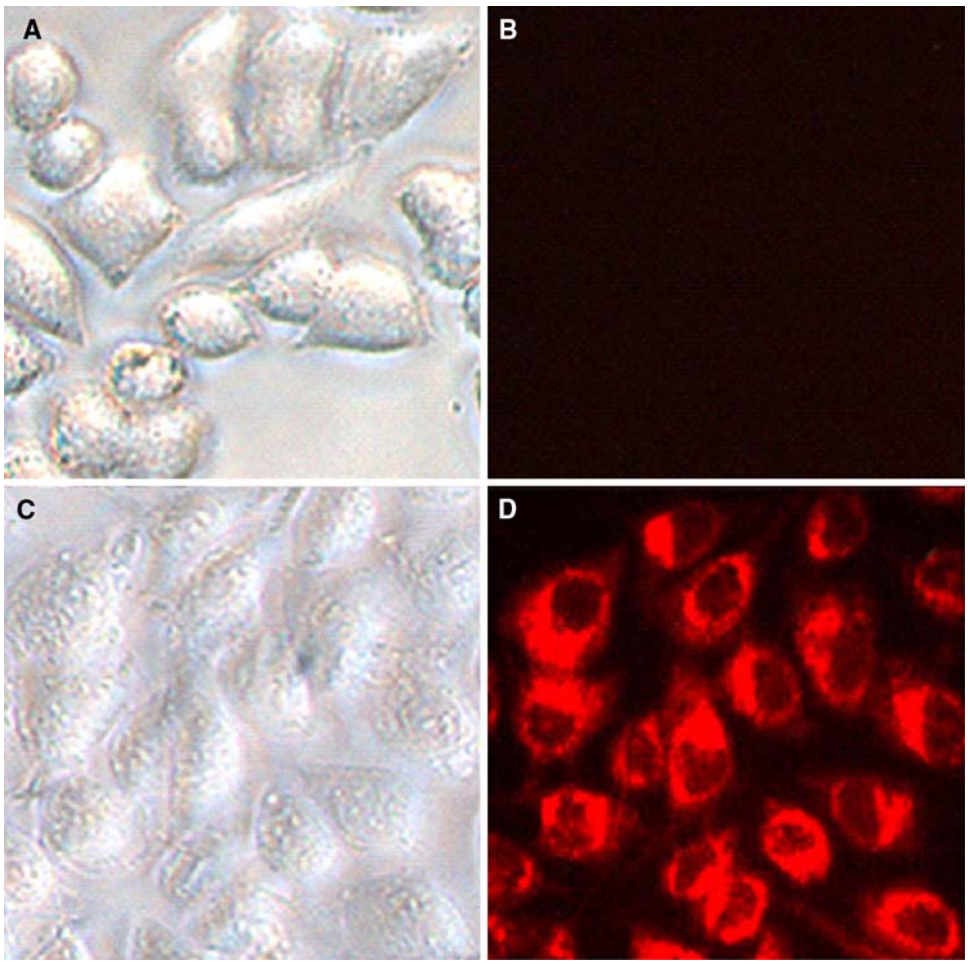

Fig. 13 Intracellular uptake of PHPP-SMNPs. Cells alone (**a**, **b**), and cells incubated with 50 μmol L^{-1} PHPP-SMNPs for 4 h (**c**, **d**)

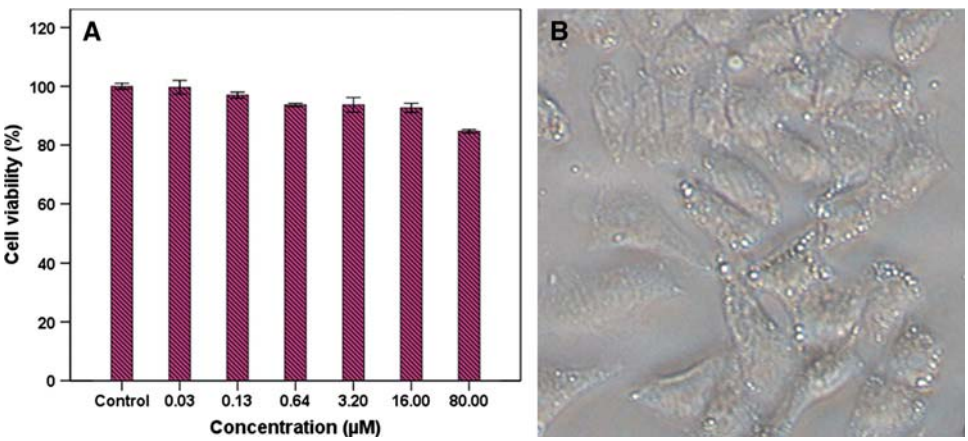

Fig. 14 Dark cytotoxicity of PHPP-SMNPs. SW480 cells were incubated with 0–80 μmol L^{-1} PHPP-SMNPs for 24 h at 37 °C in the dark. Cell toxicity was determined by MTT assay. Data represent mean ± SD ($n = 3$)

Cell viability was normalized to control cells (no drug and unirradiated) in Fig. 14. The combination of 24 h exposure of tumor cells to PHPP-SMNPs and 4.35 J/cm^2 irradiation induced a drug concentration-dependent cytotoxicity to SW480 tumor cells, which was significantly different from unirradiated control in statistics, as shown in Fig. 15. With a 10 min light exposure, 80 μmol L^{-1} PHPP-SMNPs in the safety range measured as above caused approximately 40% cell viability lost, demonstrating obvious photodynamic activity. The group treated with the drug without light exposure showed that the drug alone had no effects on tumor cells which coincided with the result of biosafety assay. In this case, the cell viability at the maximum of concentration (80 μmol L^{-1}), slightly lower than the control, was caused by the natural light during the execution of experiments.

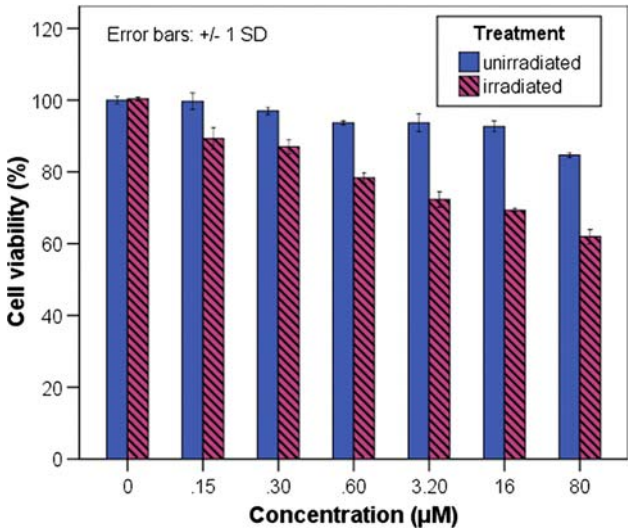

Fig. 15 In vitro photodynamic activity of PHPP-SMNPs. SW480 cells were incubated with 0–80 μmol L^{-1} PHPP-SMNPs for 24 h at 37 °C in the dark prior to irradiation for 10 min (4.35 J/cm^2) with 488-nm argon-ion laser (4.35 J/cm^2) from the underside of the culture plate. Cell viability was determined by MTT assay. Data represent mean ± SD ($n = 3$). Comparisons between two groups were made by unpaired two tailed Student's *t*-test using SPSS 15.0 software

Conclusions

Novel multifunctional silica-based magnetic nanoparticles containing photosensitizer PHPP were prepared. The PHPP-SMNPs were approximately spherical and 20–30 nm in diameter, achieving 20.8% encapsulation efficiency of PHPP. They showed no obvious toxicity without irradiation, but significant generation of singlet oxygen and remarkable photodynamic efficacy after irradiation. The PHPP-SMNPs were primarily distributed in the cytoplasm.

It can be concluded that the silica-based magnetic nanoparticles are of great value as effective drug delivery system in targeting photodynamic therapy. The potential of the magnetic core for magnetic resonance imaging and magnetic hyperthermia therapy could also be expected.

Acknowledgments This work was supported by National Natural Science Foundation of China (grant nos. 30070862, 30271534), Shanghai Municipal Foundation (grant nos. 05ZR14002, 06PJ14001, 064319020).

References

1. J. Levy, M. Obochi, Photochem. Photobiol. **64**, 737 (1996). doi:10.1111/j.1751-1097.1996.tb01828.x
2. Y. Konan, R. Gurny, E. Allémann, J. Photochem. Photobiol. B **66**, 89 (2002)
3. T. Dougherty, Photochem. Photobiol. **45**, 879 (1987). doi:10.1111/j.1751-1097.1987.tb07898.x
4. I. Roy, T. Ohulchanskyy, H. Pudavar, E. Bergey, A. Oseroff, J. Morgan, T. Dougherty, P. Prasad, J. Am. Chem. Soc. **125**, 7860 (2003). doi:10.1021/ja0343095
5. S. Wang, R. Gao, F. Zhou, M. Selke, J. Mater. Chem. **14**, 487 (2004). doi:10.1039/b311429e
6. R. De Gao, H. Xu, M. Philbert, R. Kopelman, Nano Lett. **6**, 2383 (2006). doi:10.1021/nl0617179
7. C. van Nostrum, Adv. Drug Deliv. Rev. **56**, 9 (2004). doi:10.1016/j.addr.2003.07.013
8. A. Derycke, P. de Witte, Adv. Drug Deliv. Rev. **56**, 17 (2004). doi:10.1016/j.addr.2003.07.014
9. J. Snyder, E. Skovsen, J. Lambert, P. Ogilby, J. Am. Chem. Soc. **127**, 14558 (2005). doi:10.1021/ja055342p
10. T. Jain, I. Roy, T. De, A. Maitra, J. Am. Chem. Soc. **120**, 11092 (1998). doi:10.1021/ja973849x
11. T.K. Jain, M.K. Reddy, M.A. Morales, D.L. Leslie-Pelecky, V. Labhasetwar, Mol. Pharm. **5**, 316 (2008). doi:10.1021/mp7001285
12. A. Quarta, R. Di Corato, L. Manna, A. Ragusa, T. Pellegrino, IEEE Trans. Nanobiosci. **6**, 298 (2007). doi:10.1109/TNB.2007.908989
13. S. Corr, Y. Rakovich, Y. Gun'ko, Nanoscale Res. Lett. **3**, 87 (2008). doi:10.1007/s11671-008-9122-8
14. C.W. Lai, Y.H. Wang, C.H. Lai, M.J. Yang, C.Y. Chen, P.T. Chou, C.S. Chan, Y. Chi, Y.C. Chen, J.K. Hsiao, Small **4**, 218 (2008). doi:10.1002/smll.200700283
15. L.O. Cinteza, T.Y. Ohulchanskyy, Y. Sahoo, E.J. Bergey, R.K. Pandey, P.N. Prasad, Mol. Pharm. **3**, 415 (2006). doi:10.1021/mp060015p
16. D. Tada, L. Vono, E. Duarte, R. Itri, P. Kiyohara, M. Baptista, L. Rossi, Langmuir **23**, 8194 (2007). doi:10.1021/la700883y
17. Z.-L. Chen, W.-Q. Wan, J.-R. Chen, F. Zhao, D.-Y. Xu, Heterocycles **48**, 1739 (1998)
18. Z.-L. Chen, W.-Q. Wang, K. Fan, Y. Zhou, W. Liu, D. Xu, Chin. J. Med. Chem. **8**, 1 (1998)
19. X. Zhou, S. Ni, X. Wang, F. Wu, Curr. Nanosci. **3**, 259 (2007). doi:10.2174/157341307781422942
20. D. Kim, S. Lee, K. Kim, M. Lee, Y. Lee, Curr. Appl. Phys. **6**, 242 (2006)
21. S. Khalafalla, G. Reimers, U.S. Patent No 3, 1974
22. L. Ramirez, K. Landfester, Macromol. Chem. Phys. **204**, 22 (2003). doi:10.1002/macp.200290052
23. R. Alex, R. Bodmeier, J. Microencapsul. **7**, 347 (1990). doi:10.3109/02652049009021845
24. B. Paul, S. Moulik, Curr. Sci. **80**, 990 (2001)
25. W. Stober, A. Fink, E. Bohn, J. Colloid Interface Sci. **26**, 62 (1968). doi:10.1016/0021-9797(68)90272-5
26. J. Kim, J.E. Lee, J. Lee, J. Yu, B. Kim, K. An, Y. Hwang, C. Shin, J. Park, J. Am. Chem. Soc. **128**, 688 (2006). doi:10.1021/ja0565875
27. I. Kraljic, S. Mohsni, Photochem. Photobiol. **28**, 577 (1978). doi:10.1111/j.1751-1097.1978.tb06972.x
28. J. Inbaraj, M. Vinodu, R. Gandhidasan, R. Murugesan, M. Padmanabhan, J. Appl. Polym. Sci. **89**, 3925 (2003). doi:10.1002/app.12610
29. Y. Choi, R. Weissleder, C. Tung, Cancer Res. **66**, 7225 (2006). doi:10.1158/0008-5472.CAN-06-0448
30. T. Mosmann, J. Immunol. Methods **65**, 55 (1983). doi:10.1016/0022-1759(83)90303-4